Modelling the size distribution and bioaccumulation of gold nanoparticles under mixture exposure

Li, Y.; Wang, X.; Liang, D.; Zhao, X.; Dong, Z.; Bai, Y.; ... ; Fan, W.

Aquatic Toxicology 280 (2025) 107286

Contents lists available at ScienceDirect

Aquatic Toxicology

journal homepage: www.elsevier.com/locate/aqtox

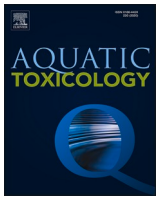

Modelling the size distribution and bioaccumulation of gold nanoparticles under mixture exposure

Yao Li [a], Xiangrui Wang [a], Dingyuan Liang [a], Xiaoli Zhao [b], Zhaomin Dong [a], Yingchen Bai [b], Wen-Xiong Wang [c], Willie J.G.M. Peijnenburg [d,e], Ying Wang [a,*], Wenhong Fan [a,*]

[a] School of Materials Science and Engineering, Beihang University, Beijing, 100191, China
[b] State Key Laboratory of Environmental Criteria and Risk Assessment, Chinese Research Academy of Environmental Sciences, Beijing, 100012, China
[c] School of Energy and Environment and State Key Laboratory of Marine Pollution, City University of Hong Kong, Kowloon, Hong Kong, China
[d] Institute of Environmental Sciences (CML), Leiden University, 2300 RA Leiden, the Netherlands
[e] National Institute of Public Health and the Environment (RIVM), Center for Safety of Substances and Products, 3720 BA Bilthoven, the Netherlands

ARTICLE INFO

Keywords:
Nanoparticles
Single-particle ICP-MS
Size distribution
Expectation–maximization algorithm
Tetrahymena thermophila

ABSTRACT

To assess the bioaccumulation and toxicity of nanoparticles (NPs), analyzing and modelling the relationship between the size distribution of NPs in organisms and the exposure particle size distribution represents an important challenge. Previous studies mostly focused on the NPs with single size. However, the size distribution of NPs is wide and variable in the natural environment. There is a lack of research on the NPs with mixed sizes. This study investigated the size distribution of three gold (Au) NPs with different sizes and their mixtures within a ciliate *Tetrahymena thermophila* under the same number concentration of particles. Results revealed that smaller particles tended to aggregate and bioaccumulate more in cells. Using expectation–maximization algorithm, a particle size distribution model of NPs in cells was established. This model effectively simulated the size distribution of NPs with mixed sizes in cells, demonstrating high accuracy with a mean absolute error of < 0.001, a root mean squared error of < 0.001, and a correlation coefficient exceeding 0.98. Experimental results further verified that the model reliably predicted the size distribution of NPs with mixed sizes in cells, and smaller particles accounted for a larger proportion of the size distribution and bioaccumulation. These results demonstrated the importance of particle size and size distribution of NPs in their environmental effects. Models developed here can provide guidance for future evaluation of the environmental risks of NPs mixtures.

1. Introduction

Engineered nanoparticles (NPs) are inevitably released into the environment due to their wide applications in many sectors (Santás-Miguel et al., 2023; Wu et al., 2020). Various NPs, such as titanium dioxide NPs, silver NPs have been detected at concentrations up to μg/L in natural environment around the world (Markus et al., 2018; Xiao et al., 2019). Given existing studies have well illustrated that the NPs may trigger toxicities to organisms, exposure to NPs may pose potential risk to organisms and environment (Batley et al., 2013; Peijnenburg et al., 2015). Addressing the risk of NPs require the understanding on the accumulation of NPs in organisms, which are significantly affected by the physicochemical properties of NPs, especially particle size (Ganguly et al., 2018; Zhu et al., 2013). As reported, the cellular interaction, absorption, metabolism, and distribution of NPs in organisms depend on the particle size distribution of NPs (Eker et al., 2024).

Many studies have already reported how single particle size affected the bioaccumulation and toxicity of NPs, and found that it was related to the distribution, fate, and interaction mechanisms of NPs in organisms (Feng et al., 2017). For example, smaller NPs with a larger surface area were more easily adsorbed on the cell surface and directly penetrated the cell wall and membrane (Chen et al., 2019). Therefore, smaller NPs were more ingested and accumulated, leading to more significant oxidative damage and metabolic toxicity (Wray and Klaine, 2015; Zhang and Wang, 2019). The surface energy and surface activity of NPs were also size-dependent and directly affected the physical adsorption, ionic bonding, covalent bonding, and aggregation of NPs, ultimately affecting the elimination, distribution, bioaccumulation, and toxicity of NPs (Cross et al., 2019; Zhu et al., 2013). These studies have sufficiently

* Corresponding authors.
E-mail addresses: yingw@buaa.edu.cn (Y. Wang), fanwh@buaa.edu.cn (W. Fan).

https://doi.org/10.1016/j.aquatox.2025.107286
Received 28 November 2024; Received in revised form 5 February 2025; Accepted 8 February 2025
Available online 11 February 2025

explored the impact of size on the bioaccumulation and toxicity of NPs by setting different single particle size treatment groups. However, the size distribution of NPs is wide and variable in the natural environment. There is a lack of research on how the bioaccumulation and toxicity of NPs change under different particle size mixtures.

To accurately assess the impact of mixed particle size on the bioaccumulation and toxicity of NPs, it is essential to characterize and quantify their size distribution in organisms (Vidmar et al., 2018). However, it is impossible to experimentally determine the size distribution of NPs in organisms for all possible combinations of different sizes. Constructing a model to predict the size distribution of NPs with mixed sizes in biological systems is a potential solution. Mathematical models are powerful tools to analyze and unravel the general rule in experimental data of NPs (Rees et al., 2019; Summers et al., 2021). For example, a stochastic mathematical model consisting of a lattice-based random walk for the cell population and a multistage stochastic model of NPs internalization accurately derived analytic approximations of the NPs dosage distribution, and showed that NPs dosage can be described by a Poisson mixture distribution with rate parameters that are a function of Beta-distributed random variables (Dowling et al., 2022). A numerical model obtained by simultaneously solving the energy equation, solute conservation equation, and the NPs transport equation predicted the effect of NPs size and local interface movement velocity on NPs engulfment (Jegatheesan and Bhattacharya, 2023). The free-volume theory was previously successfully used to explore the influence of NPs crowding on polymer shapes (Lim and Denton, 2014). Therefore, combining mathematical models with experimental data provides the possibility to predict the size distribution of NPs, which can be validated through statistical comparison of the predicted and experimental results (McColl et al., 2014).

In order to investigate and model the size distribution of NPs with different sizes and their mixtures, we firstly analyzed the size distribution of NPs with a single size in organisms by single-particle inductively coupled plasma mass spectrometry (spICP-MS), and then established a mathematical model to simulate the size distribution of NPs with mixed sizes in organisms. The ciliate, *Tetrahymena thermophila* (*T. thermophila*) was selected as the model organism because they can uptake NPs non-selectively (Mortimer et al., 2011; Rajapakse et al., 2016). Gold (Au) NPs, a chemically stable NPs (Avellan et al., 2018), were selected as the model NPs. A mixture size distribution model based on the expectation–maximization (EM) algorithm was established. The model reliably simulated the particle size distribution of Au NPs with mixed sizes in cells, which enabled a more convenient estimation of the bioaccumulation, toxicity, and environmental risks of NPs.

2. Materials and methods

2.1. Synthesis and characterization of Au NPs

Au NPs were prepared according to the method reported by Gao et al., 2012. Detailed information is given in Text S1 (Supplementary Material). Three sizes of polyvinylpyrrolidone (PVP)-coated Au NPs (30, 70, and 140 nm) were used. The synthesized Au NPs were characterized by scanning electron microscope (SEM) with an operating voltage of 8.00 kV (ZEISS Sigma 500, Carl Zeiss, Germany). Au NPs suspensions were characterized by dynamic light scattering (DLS), and their zeta potentials were determined in triplicate (Nano ZS-ZEN3600, Malvern, England). The mass concentration of Au NPs in stock suspension was measured by ICP-MS (NexION 350D, Perkin Elmer, America). Prior to use, the suspensions were sonicated for 15 minutes to ensure the particles did not aggregate in the exposure medium.

2.2. Exposure assays

T. thermophila SB210 were obtained from the Institute of Hydrobiology, Chinese Academy of Sciences, Wuhan. After a 48-hour culture (Text S2, Supplementary Material), *T. thermophila* in the logarithmic phase were centrifuged at 2500 rpm for 5 minutes and washed twice with fresh water. The precipitate was then resuspended in freshwater to obtain 1×10^6 cells/mL for subsequent experiments, determined using a Z2 Coulter counter (Beckman Coulter, America). The exposure medium was prepared by adjusting the Au NPs in the stock suspension to a specific particle concentration based on the mass concentration and size distribution, determined by ICP-MS and SEM measurements, respectively. The cells were mixed with an equal volume of exposure medium to obtain a final concentration of 5×10^5 cells/mL and 6.8×10^7 particles/mL (Table 1). *T. thermophila* were exposed to the same number of Au NPs of three sizes for 6 hours to ensure equilibrium was reached between the Au NPs and cells in subsequent experiments (Wang et al., 2019). Freshwater-exposed cells were used as the control.

2.3. Sample extraction and spICP-MS analysis

Following a 6-hour exposure period, the cell pellets were collected after centrifugation (2500 rpm) for 5 minutes at 4 °C and washed three times with phosphate buffer saline (PBS, 0.1 mol/L, pH 7.5) containing 10 % v/v dimethyl sulfoxide (DMSO) (Abdolahpur Monikh et al., 2021). The unbound and loosely attached Au NPs in the supernatant were removed and the Au NPs with strong adhesion would ultimately be internalized by cells (Lesniak et al., 2013). Meanwhile, the content of Au in the supernatant was determined by ICP-MS to ensure that the cells were cleaned thoroughly. Au NPs internalized by cells were then extracted according to the method reported before (Gray et al., 2013). Specifically, cells were treated by an ultrasonic cell grinder (Scientz-IID, Ningbo Xinzhi Biotechnology Co. Ltd., China) to obtain a homogenate, which was mixed with ultrapure water and alkine tetramethylammonium hydroxide (TMAH, 25 % w/w, Shanghai Aladdin Co. Ltd., China) to a final concentration of 20 % w/w TMAH. The samples were then sonicated for 1 hour and rotated mechanically at 25 °C for 23 hours. Finally, to minimize the impact of pH increase caused by TMAH (Mohanraj et al., 2017), all samples were diluted to a final concentration of 1 % w/w TMAH and sonicated for at least 15 minutes prior to spICP-MS analysis (NexION 350D, Perkin Elmer, America). All samples were prepared in triplicate. Detailed information on the operating conditions and dissolved and particle calibrations of spICP-MS are provided in Table S1 and Figure S1 (Supplementary Material). The transport efficiency was 7.06 %, and the size detection limit was 14.80 nm.

To evaluate the effectiveness of the digestion method in this study, spiked recovery experiments were conducted using standard Au NPs with concentrations of 100 μg/kg ww and sizes of 20, 50, and 80 nm (Nanopartz, America). After pipetting standard Au NPs solutions onto control cell pellets, sample extraction and analysis were as described previously. This method achieved recovery rates of 92.7 ± 0.3 %, 115 ± 3 %, and 122 ± 2 % for the 20, 50, and 80 nm Au NPs, respectively, and the impact of pH increase on the NPs size was effectively controlled, as the variation range of the size distribution was < 10 % (Figure S2, Supplementary Material).

Table 1
The size and number concentration of Au NPs in each exposure group.

Group	A	B	C	A + B	A + C	B + C	A + B + C
30 nm (particles/mL)	6.8×10^7	–	–	6.8×10^7	6.8×10^7	–	6.8×10^7
70 nm (particles/mL)	–	6.8×10^7	–	6.8×10^7	–	6.8×10^7	6.8×10^7
140 nm (particles/mL)	–	–	6.8×10^7	–	6.8×10^7	6.8×10^7	6.8×10^7

2.4. The bioaccumulation metrics of NPs

In this study, the concentration factor (CF) was chosen to evaluate the bioaccumulation of Au NPs in *T. thermophila*. The CF described the ratio between the body burden of a substance (mg/kg dw) taken up from the surrounding medium (water) and the exposure concentration (mg/L) (Arnot and Gobas, 2006). 1860 pg/cell was used as the cellular dry weight of *T. thermophila* (Mortimer et al., 2016).

The CF (L/g dw) value was calculated by Eq. (1):

$$\mathrm{CF} = \frac{C_{\mathrm{organism}}}{C_{\mathrm{water}}} \tag{1}$$

where C_{organism} and C_{water} represent the Au mass concentration in *T. thermophila* (mg/g dw) and the exposure medium (mg/L), respectively. C_{organism} and C_{water} were obtained by ICP-MS after digesting *T. thermophila* and exposure medium with aqua regia (V (37 % HCl): V (68 % HNO_3) = 3:1), respectively.

The number concentration factor (NCF, mL/g dw) was used to evaluate the number concentration change of Au NPs in *T. thermophila* by Eq. (2):

$$\mathrm{NCF} = \frac{N_{\mathrm{organism}}}{N_{\mathrm{water}}} \tag{2}$$

where N_{organism} and N_{water} represent the number concentration of Au NPs in *T. thermophila* (particles/g dw) and the exposure medium (particles/mL), respectively.

2.5. EM algorithm-based mixture size distribution model

In general, the size distribution of NPs is continuous (Ali-zade, 2008). Any continuous distribution can be well approximated by an appropriate finite mixture of a normal distributions model (Xu and Knight, 2010). The finite mixture of normal distributions model is a mixed distribution composed of K different normal distributions, which can be used to represent the probability distribution of observed data in a population (Quandt and Ramsey, 1978). The mixture of normal distribution models is widely acknowledged as flexible and powerful probabilistic modelling tools for univariate and multivariate data since they can capture the leptokurtic, skewed, and multimodal characteristics of empirical data (Quandt and Ramsey, 1978). Various methods have been proposed and are used for estimating the unknown parameters in the mixed normal distributions models, of which the maximum likelihood estimation is one of the most popular because of its asymptotic statistical properties (Xu and Knight, 2010). The EM algorithm is the standard method used to fit mixtures of normal distributions model to observed data, which converge to a maximum likelihood (ML) estimate of the mixture parameters (Xu and Jordan, 1996). Therefore, predicting the size distribution of NPs in organisms by mixtures of normal distribution models and EM algorithm is an appropriate method.

2.5.1. Mixtures of normal distributions model based on EM algorithm

The mixture of normal distributions model is a hybrid distribution obtained by a linear combination of multiple single normal distribution models, with the restriction of the sum of the weight coefficients of each single model being equal to 1 (Wang and Taaffe, 2015). This approach has the advantages of simple structure, flexible shape, and good fitting performance. Moreover, this model is based on the minimum fitting error index, which can better describe the particle size distribution of Au NPs in cells.

Let $x_1, x_2, \ldots, x_n$ denote a sequence sample of particle size of Au NPs in cells (nm) data of independent identically distributed random variables with an unknown probability density function $f(x)$. The probability density function of $f(x)$ is considered as a mixture of normal distributions model with K components, which can be expressed as follows:

$$f(x|\theta) = \sum_{i=1}^{\mathrm{K}} \lambda_i \phi(x|\theta_i) \Bigg) \tag{3}$$

where θ is the optimal model parameter, for which $\theta = (\widetilde{\lambda_i}, \widetilde{\mu_i}, \widetilde{\theta_i})$, λ_i is the probability that the observation data belong to the i^{th} normal distribution, and $\sum_{i=1}^{\mathrm{K}} \lambda_i = 1$, $\lambda_i \geq 0$, $\phi(x|\theta_i)$ is the probability density function of i^{th} normal distribution, $\theta_i = (\mu_i, \sigma_i^2)$, and μ_i is the mean value and the location parameter, and σ_i is the standard deviation and the scale parameter.

The EM algorithm is an iterative algorithm that alternates between guessing a probability distribution over completions of missing data given the current model (the E-step) and re-estimating the model parameters using these completions (the M-step) (Dempster et al., 1977; Do and Batzoglou, 2008). The steps for updating the mixed normal distributions model parameters, λ_i, μ_i, and σ_i, through the EM algorithm are as follows (Quandt and Ramsey, 1978):

(1) Define the value of K, which equals to 2 or 3 in this study. Set the initial value for each unknown parameters λ_i, μ_i, and σ_i, and calculate the logarithmic likelihood function $\log \mathrm{h}(\theta)$ of Eq. (4):

$$\log \mathrm{h}(\theta) = \log f(x|\theta) = \sum_{i=1}^{n} \log \sum_{k=1}^{\mathrm{K}} \lambda_k \phi(x_k|\theta_k),\ i = 1, \cdots, n \text{ and } k = 1, \cdots, \mathrm{K} \tag{4}$$

(2) The E-step: Calculate the "posterior" probabilities (conditional on the original particle size distribution and the current value of parameters λ_i, μ_i, and σ_i) of component inclusion by Eq. (5):

$$\gamma_{ik} = \frac{\lambda_k \phi(x_i|\theta_k)}{\sum_{k=1}^{\mathrm{K}} \lambda_k \phi(x_i|\theta_k)} \tag{5}$$

where γ_{jk} is the posterior probability of data j from sub model k, $\phi(x_j|\theta_k)$ is the probability density function of k^{th} normal distribution, and $\theta_k = (\mu_k, \sigma_k^2)$, $i = 1, \ldots, n$, $k = 1, \ldots, \mathrm{K}$.

(3) The M-step: Calculate the parameters λ_i, μ_i, and σ_i after a new round of iteration:

$$\lambda_k{}^{\mathrm{new}} = \frac{1}{n} \sum_{i=1}^{n} \gamma_{ik},\ \text{for } k = 1, \cdots, \mathrm{K} \tag{6}$$

$$\mu_k{}^{\mathrm{new}} = \frac{\sum_{i=1}^{n} (\gamma_{ik} x_i)}{\sum_{i=1}^{n} \gamma_{ik}},\ \text{for } k = 1, \cdots, \mathrm{K}. \tag{7}$$

$$\sigma_k{}^{2\ \mathrm{new}} = \frac{\sum_{i=1}^{n} \gamma_{ik} (x_i - \mu_k{}^{\mathrm{new}})(x_i - \mu_k{}^{\mathrm{new}})^T}{\sum_{i=1}^{n} \gamma_{ik}},\ \text{for } k = 1, \cdots, \mathrm{K}. \tag{8}$$

(4) Repeat the E-step and M-step calculations until parameters or likelihood functions of Eq. (4) converge.

These calculation and modelling processes were realized by the mix tools package in the R 3.5.2 software, which provided a set of functions for analyzing a variety of infinite mixture models (Benaglia et al., 2009).

2.5.2. Model evaluation

The mean absolute error (MAE), root mean squared error (RMSE), and correlation coefficient (ρ) between the predicted and experimental results were used to evaluate the EM algorithm-based mixture size distribution model in this study (Eqs. (9)-(12)). MAE and RMSE can quantify the deviation between predicted and experimental results with smaller values indicating better precision of the model. ρ can represent the linear correlation between predicted and experimental results. The accuracy of the model is higher when the ρ value is closer to 1 (Ma et al., 2022).

$$E_i = Y_i' - \overline{Y_i} \tag{9}$$

$$\mathrm{MAE} = \frac{1}{n}\sum_{i=1}^{n}|E_i| \tag{10}$$

$$\mathrm{RMSE} = \sqrt{\frac{1}{n}\sum_{i=1}^{n}E_i^2} \tag{11}$$

$$\rho = \frac{cov(P_1, P_2)}{\sqrt{D(P_1)}\sqrt{D(P_2)}} \tag{12}$$

where $i = 1, 2, \ldots, m$, m is the array of frequency distribution histograms, $\bar{Y}_i$ is the ordinate value of the i^{th} histogram, Y_i' is the corresponding function value of the fitted probability density curve, n is the number of sample sequences, P is the observed value of a sequence sample, cov is the covariance, and D is the variance.

2.6. Data analysis

Results were expressed as mean value ± standard deviation ($n = 3$). To conduct statistical analyses of the data, SPSS software (IBM SPSS Statistics 19.0) was employed. Pearson correlation coefficient (r) was calculated to evaluate the extent of the linear relationship between two variables.

3. Results and discussion

3.1. Characterization of Au NPs

The particle shape, size distribution, hydrodynamic diameter, and zeta potential of three Au NP suspensions were characterized. As illustrated, the Au NPs were spherical and monodispersed (Fig. 1). The mean diameters of A, B, and C were 29 ± 4 nm, 67 ± 13 nm, and 143 ± 28 nm, respectively. The hydrodynamic size and size distribution were measured by DLS (Figure S3, Supplementary Material), with hydrodynamic diameters of 68.3 ± 0.15, 107.4 ± 0.54, and 176 ± 1 nm, and polydispersity indexes (PDI) of 0.32 ± 0.02, 0.16 ± 0.01, and 0.071 ± 0.018, for A, B, and C, respectively. The zeta potentials were −31.9 mV, −0.03 mV, and +0.27 mV for A, B, and C, respectively.

3.2. Size distribution of Au NPs in T. thermophila

As illustrated, Au NPs were monodispersed (Fig. 1b). However, the size distributions in *T. thermophila* were relatively evenly dispersed, with a slight right skew (Fig. 2a), demonstrating that Au NPs aggregated into larger particles with different particle sizes in *T. thermophila*. Excluding the minor influence of particle size increase during the extraction process, the mean and deviation values of the size distribution of all Au NPs in *T. thermophila* were much larger than the exposure size distribution, suggesting strong aggregation of Au NPs. In addition, the average size increased to 495 % of group A, 184 % of group B, and 130 % of group C in cells with increasing exposure particle size. The size distributions in cells (Fig. 2a) were wider than the exposure size distributions (Fig. 1b).

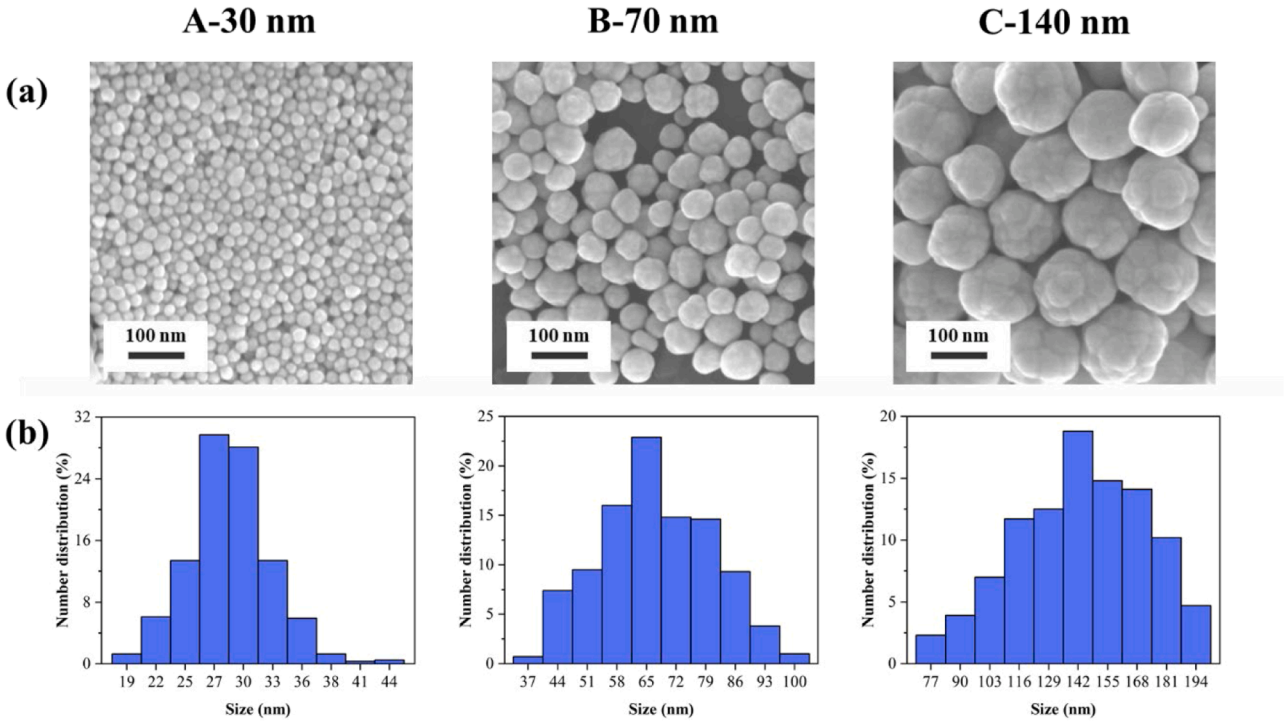

Fig. 1. Characterization of gold nanoparticles (Au NPs). (a) Scanning electron microscope (SEM) images of the Au NPs with different sizes. (b) Size distributions of Au NPs according to the SEM images, with 606 NPs for particle A, 419 NPs for particle B, and 128 NPs for particle C.

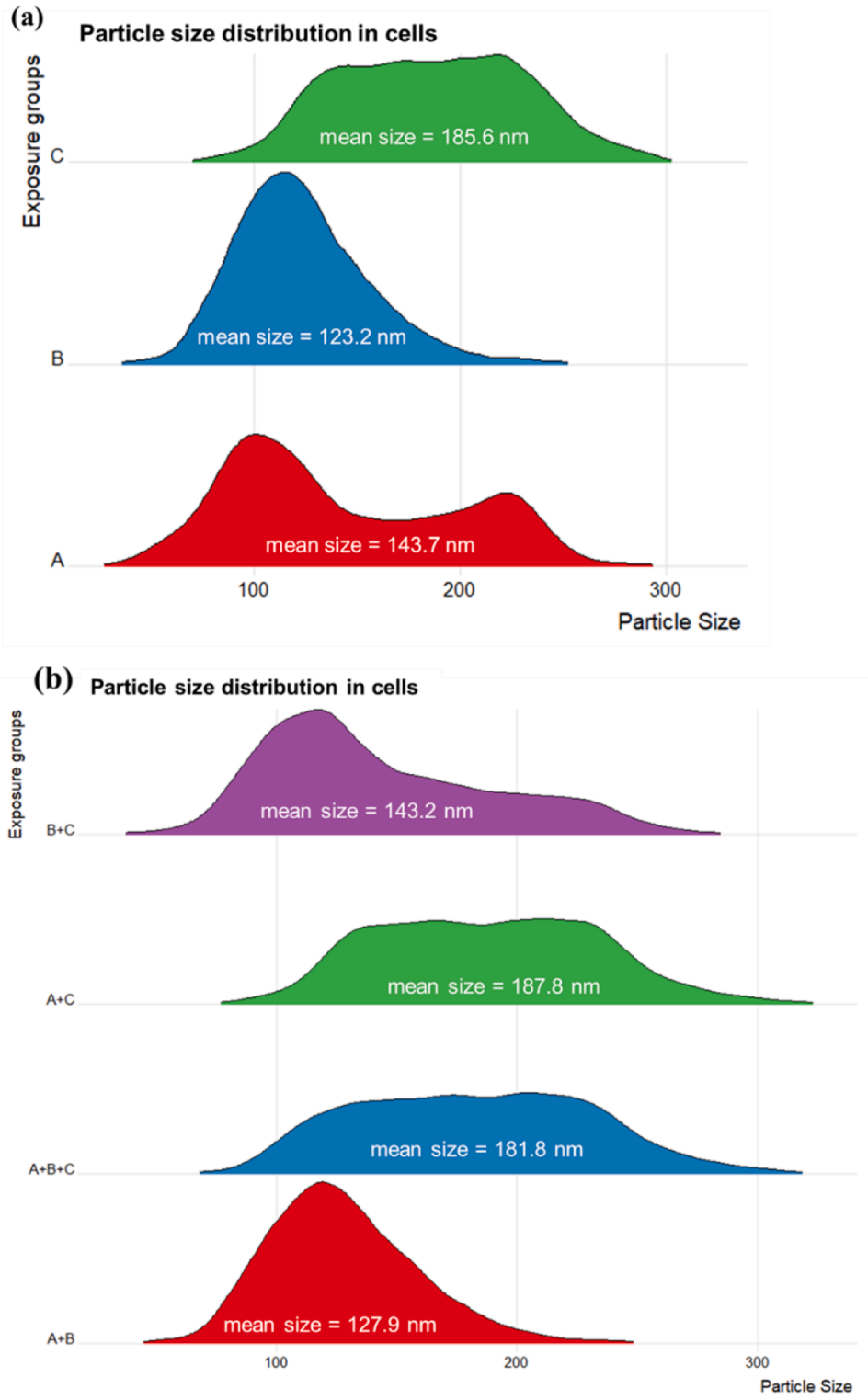

Fig. 2. The size distribution of Au NPs with (a) single size and (b) mixed sizes in cells. The size distribution was measured by single-particle inductively coupled plasma mass spectrometry (spICP-MS), where the area under the curves is equal to 1.

These findings indicated that Au NPs aggregated after ingestion by *T. thermophila*, with the smallest Au NPs (i.e., group A with 30 nm particles) showing the most significant aggregation in cells. NPs had a large volume-specific surface area and a high surface energy, making them susceptible to agglomeration to diminish their surface area and energy (Gatoo et al., 2014). Smaller NPs had a larger volume-specific surface area and higher surface energy (Abdolahpur Monikh et al., 2019), which further enhanced particle aggregation to form larger stable particles.

The size distributions of NPs with mixed sizes in *T. thermophila* were relatively evenly dispersed with a slight right skew (Fig. 2b). Au NPs with mixed sizes also aggregated in *T. thermophila*. The average size increased to 266 % of group A + B, 228 % of group A + B + C, and 218 % of group B + C in *T. thermophila* with increasing exposure particle size,

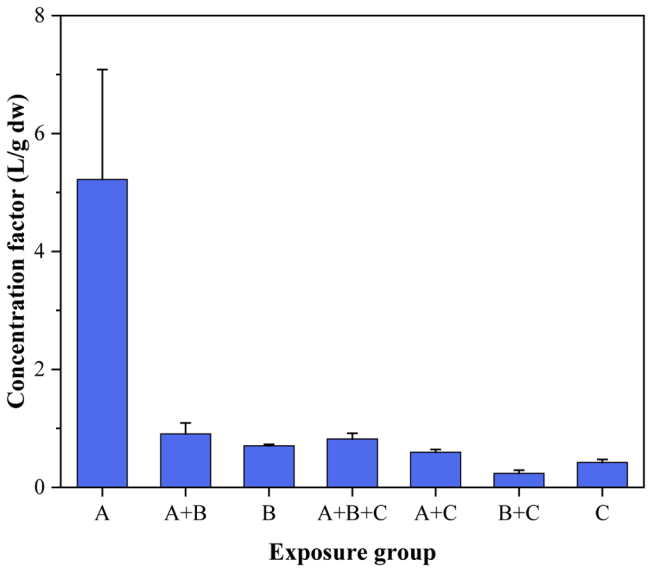

Fig. 3. The concentration factor (CF) values on all exposure groups. The correlation coefficient between CF and exposure particle size was -0.674, p = 0.097. The data presented represents the mean ± standard deviation (n = 3).

which also indicated that smaller NPs were more likely to aggregate.

3.3. Au NPs bioaccumulation in T. thermophila

As described in Section 2.3, the content of Au in the removed supernatant during the cell cleaning process was 0.008 ± 0.004 μg/L. This ensured that unbound and loosely attached Au NPs were thoroughly cleaned, and only the Au NPs internalized by the cells were ultimately detected (Lesniak et al., 2013). The CF was further calculated to evaluate the bioaccumulation of Au NPs in *T. thermophila* (Fig. 3 and Table S2, Supplementary Material). The CF value of group A was significantly higher than that of other groups. The CF values decreased first and then tended to remain unchanged with increasing exposure particle size, indicating the size-dependent bioaccumulation of Au NPs in *T. thermophila*. As a unicellular organism, *T. thermophila* ingested large NPs through endocytosis, while small NPs could pass directly through cell membranes, circumventing complex reactions and high energy consumption (Behra et al., 2013; Hartenstein and Martinez, 2019). Additionally, smaller particles with larger specific surface areas were more easily adsorbed due to their relatively large surface area available for direct contact between the particles and cells, and then they accumulated in cells (Chen et al., 2019; Cross et al., 2019).

3.4. Establishment of the EM algorithm-based mixture size distribution model

Using the three single size distribution results in cells and considering the randomness of NPs size, the EM algorithm-based mixture size distribution model was established to simulate the size distribution in cells when *T. thermophila* were exposed to mixtures of A, B, and C with the same particle number concentration (Fig. 4). The size distributions of mixed A, B, and C in cells were effectively simulated by the model based on the EM algorithm. The MAE and RMSE values were close to 0 and ρ was close to 1 (MAE < 0.001, RMSE < 0.001, ρ > 0.98) (Table 2 and Figure S4, Supplementary Material).

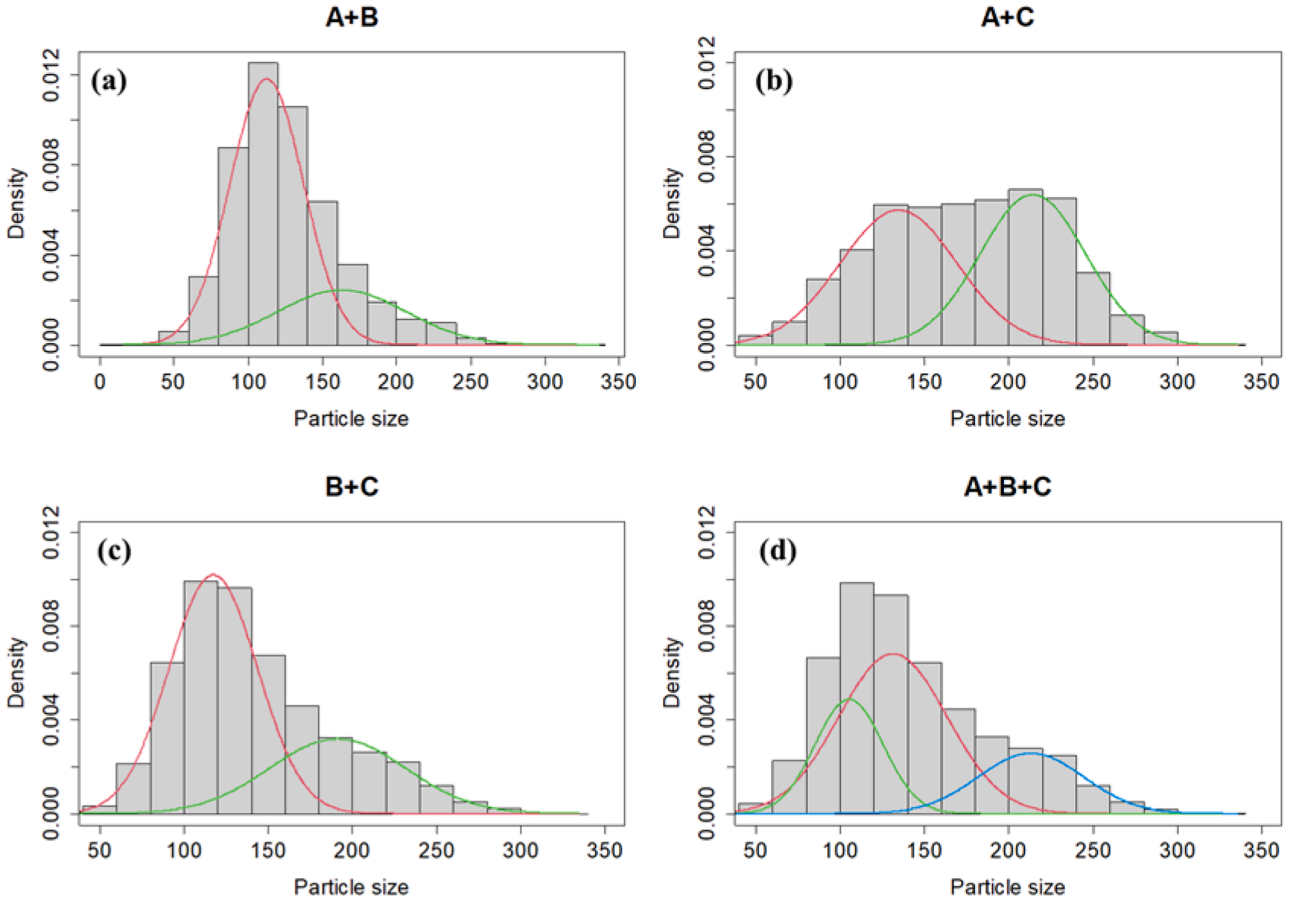

Fig. 4. Predictions of size distribution of mixed size exposure groups in cells. (a) A + B, (b) A + C, (c) B + C, and (d) A + B + C with the same concentration ratio of 1:1:1 based on the expectation–maximization (EM) algorithm and experimental results of single particle exposure groups.

Table 2
Parameters of the EM algorithm-based mixture size distribution model. Weight coefficient (λ), expectation (μ), standard deviation (σ), mean absolute error (MAE), root mean squared error (RMSE), and correlation coefficient (ρ) of EM algorithm-based mixture size distribution model.

Group	Compound 1			Compound 2			Compound 3			MAE	RMSE	ρ
	λ_1	μ_1	σ_1	λ_2	μ_2	σ_2	λ_3	μ_3	σ_3			
A + B	0.736	112.5	24.8	0.264	163.0	43.0	–	–	–	2.95×10^{-4}	5.34×10^{-4}	0.991
A + C	0.498	134.8	34.6	0.502	214.3	31.3	–	–	–	3.02×10^{-4}	4.48×10^{-4}	0.986
B + C	0.675	117.5	26.4	0.325	191.3	40.5	–	–	–	2.56×10^{-4}	4.33×10^{-4}	0.992
A + B + C	0.247	105.4	20.1	0.550	131.4	32.1	0.203	213.2	31.4	2.40×10^{-4}	4.17×10^{-4}	0.992

Note: $\Sigma\lambda_i = 1$.

The model predictions demonstrated that the size distributions of mixed sizes in cells were relatively evenly dispersed with a slight right skew (Fig. 4). This was analogous to the experimental results (Fig. 2b). The simulation showed that the smaller particle accounted for a large proportion in the mixed distribution when the particle size difference between the mixtures was small, such as A + B and B + C ($\lambda_1 > 0.6$) (Table 2). However, the results were different when the particle size difference in the mixtures was large, i.e., A + C ($\lambda_1 \approx \lambda_2$) and A + B + C ($\lambda_1 \approx \lambda_3$). The parameters μ_i and σ_i of the EM algorithm-based mixture size distribution model were different under the four exposure groups, indicating that the mixed distribution was not a simple linear combination of single size distribution. This might be due to the different degrees of aggregation of NPs in organisms with different particle sizes. Moreover, parameter σ of larger NPs in the EM algorithm-based mixture size distribution model was greater than that of smaller NPs, which might be related to the interaction forces between particles (Wang et al., 2021).

3.5. Validation of the EM algorithm-based mixture size distribution model

To evaluate and validate the EM algorithm-based mixture size distribution model, the simulated and experimental results were compared (Fig. 5 and Figure S5, Supplementary Material). The model was effective in predicting the particle size distributions of mixed size exposure groups in cells, except for the group A + B + C. The large difference between the simulated and experimental size frequency of A + B + C

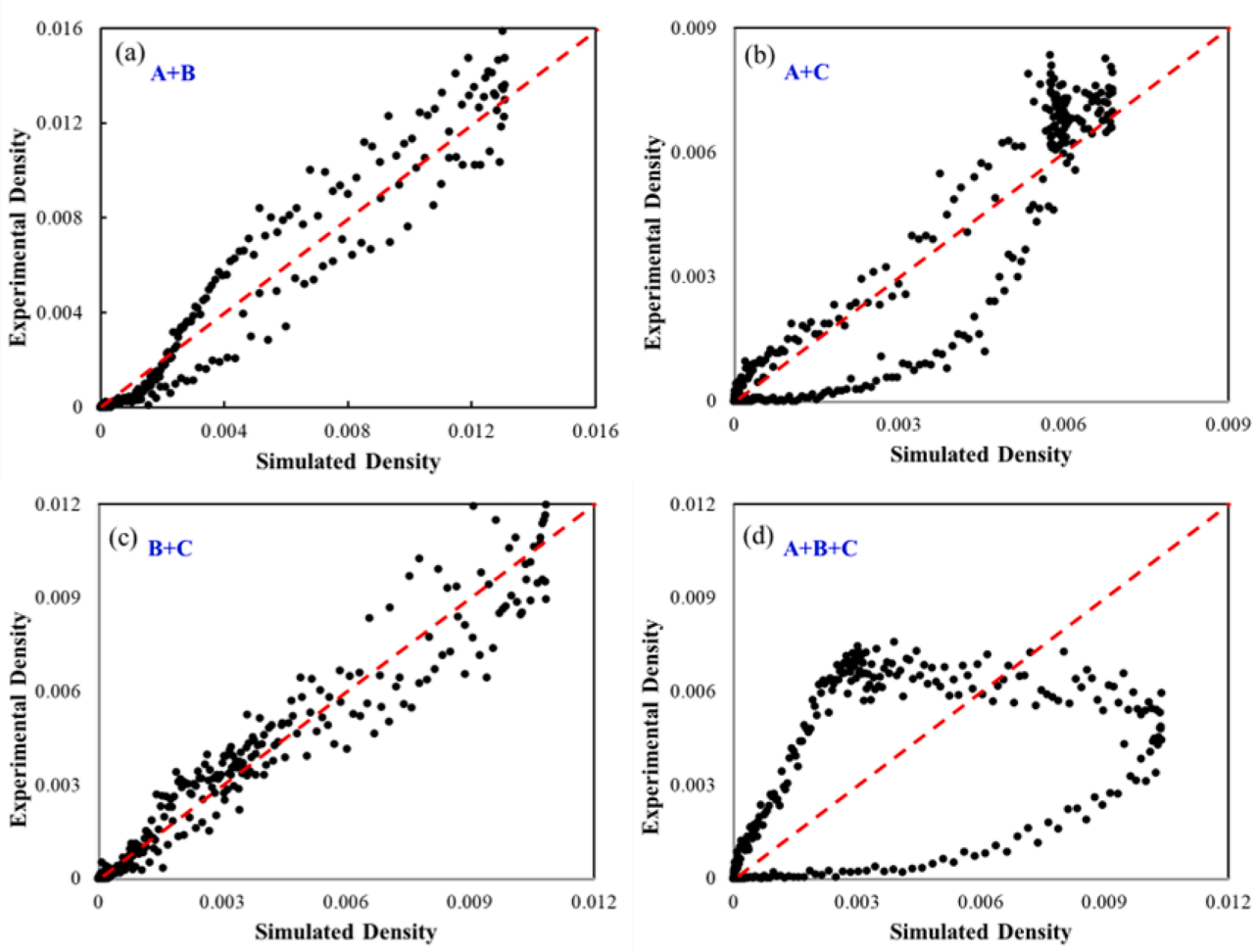

Fig. 5. Experimental validation of the mixture of normal distribution models based on the EM algorithm. Comparisons of particle size distribution frequency in cells of (a) A + B, (b) A + C, (c) B + C, and (d) A + B + C between predicted results based on the EM algorithm and experimental results of mixed particle size exposure groups. The abscissa represents the predicted results based on the EM algorithm. The ordinate represents the experimental results of mixed particle size exposure groups. The red dotted line represents the case where y equals x.

could be due to the interaction forces among the NPs. Based on classical DLVO theory (Wang et al., 2021), the interaction forces (V_T), Van der Waals forces (V_A), and electrostatic repulsion forces (V_R) between particles were calculated and simulated by R 3.5.2 software (Text S3 and Figure S6, Supplementary Material) (Benaglia et al., 2009). The interaction forces became smaller with larger particle size, so the particle system was more unstable (Sefcik et al., 2005). Therefore, the interaction forces between NPs differed more when the particle size difference increased, making the EM algorithm-based mixture size distribution model less effective.

On another aspect, the large difference between the simulated and experimental size frequency of A + B + C could also be due to the interactions between NPs and proteins. For example, the adsorption of proteins by NPs, the tertiary structure, thermodynamics and kinetic stability, and function of proteins were all affected by the particle size (Shang et al., 2009; Wang et al., 2011). Larger NPs could adsorb more proteins and change the function of proteins more effectively due to their higher surface area (García-Álvarez et al., 2018). These processes might result in differences between simulated and experimental size frequency. In the future, the EM algorithm-based mixture size distribution model needs to be further improved to correct the effect of interaction forces among NPs and between NPs and proteins.

In the EM algorithm-based mixture size distribution model, a parameter k was defined as the ratio of smaller and larger NPs in the model, and it was calculated according to Eqs. (13)-(14).

$$k = \frac{\lambda_1\mu_1}{\lambda_2\mu_2} \tag{13}$$

$$k = \frac{\lambda_1\mu_1 + \lambda_2\mu_2}{\lambda_2\mu_2 + \lambda_3\mu_3} \tag{14}$$

where λ_i is the weight coefficient that the observation data belong to the i^{th} normal distribution, μ_i is the expectation value of the i^{th} normal distribution. They were obtained by the EM algorithm-based mixture size distribution model and listed in Table 2.

The relationships among k, NCF, CF, and exposure size of NPs were analyzed (Fig. 6). There were negative correlations between the exposure size of NPs, NCF, and CF ($r = -0.963$, $p = 0.037$; $r = -0.942$, $p = 0.058$, respectively), indicating that the bioaccumulation of NPs was related to the particle size, and increased with the decrease of size. There was a positive correlation between k and NCF ($r = 0.998$, $p = 0.0016$; Fig. 6c). The NCF increased with the increase of proportion of smaller NPs, which was consistent with the relationship of exposure size of NPs and NCF. However, the CF first increased and then tended to remain unchanged with the increase of k, which was different from the relationship of exposure size of NPs and CF. The bioaccumulation of NPs

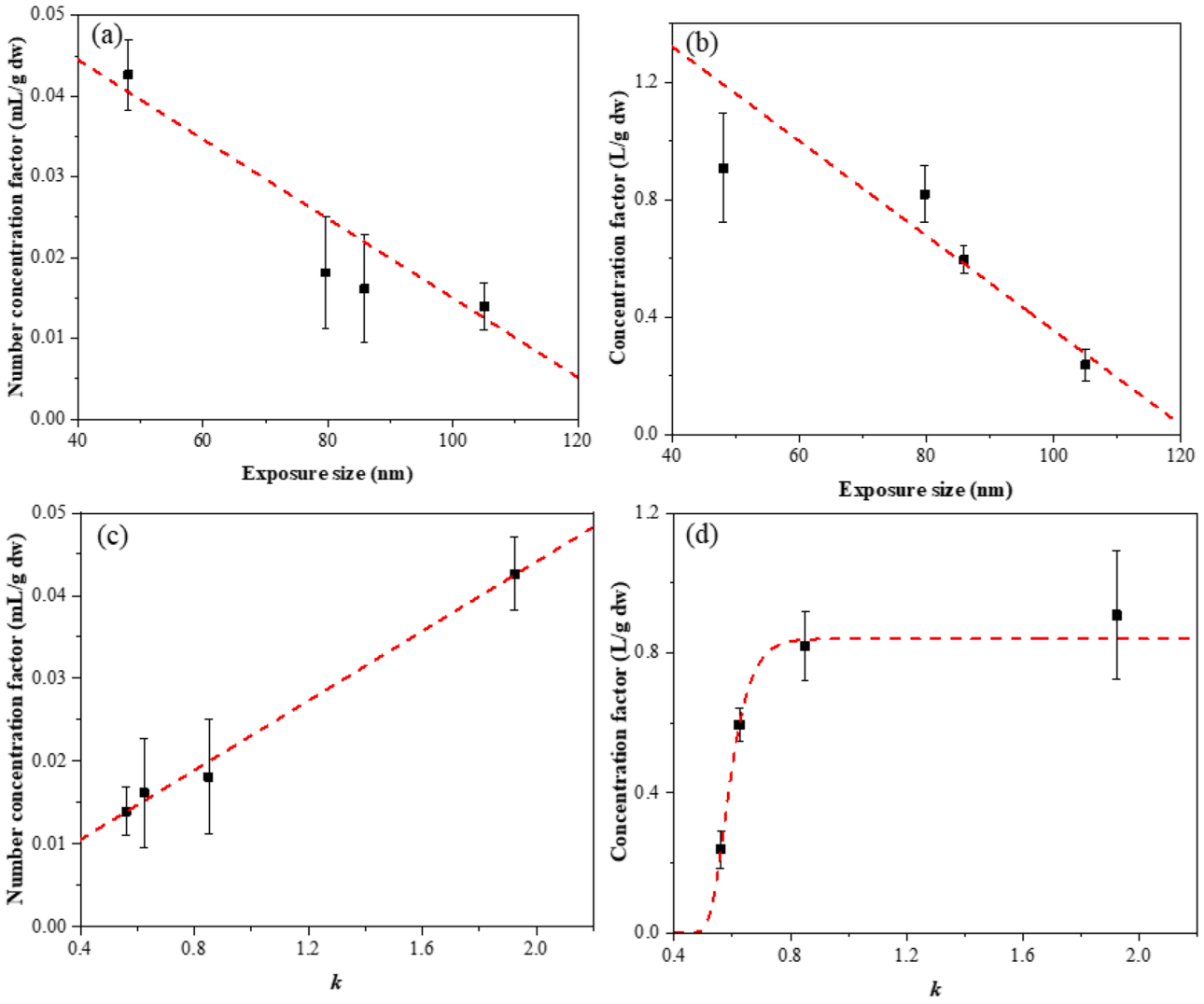

Fig. 6. Relationships between the (a) exposure size of NPs and NCF, (b) exposure size of NPs and CF, (c) k and NCF, and (d) k and CF. The data presented represents the mean ± standard deviation ($n = 3$).

tended to be saturated with the increase of proportion of smaller NPs, indicating that smaller NPs were more important in bioaccumulation. Similarly, the specific surface area of NPs, binding to cell membrane receptors, inflammatory responses, genotoxicity, developmental toxicity, and intracellular migration processes were more affected by smaller NPs (Bai et al., 2014; Park et al., 2011; Schübbe et al., 2012). Therefore, compared with the exposure size of NPs, the parameter k calculated based on the mixture size distribution model in this study described the bioaccumulation of NPs more scientifically.

4. Conclusion

This study applied spICP-MS for investigating the bioaccumulation and size distribution of NPs in organisms, established the mixture size distribution model based on EM algorithm, and effectively simulated the size distribution of Au NPs with different sizes. It is feasible to simulate and predict the size distribution of NPs based on the mixture size distribution model in the future, with the prerequisite of obtaining the basic information including types and size distributions of NPs in organisms. This study provided the foundation for further exploration of the toxicity and environmental risk of NPs with different sizes. However, further research is still needed in the following areas: (a) correct the effect of interaction forces among NPs and between NPs and proteins on the EM algorithm-based mixture size distribution model, and the interaction forces can be investigated using atomic force microscopy, quartz crystal microbalance, molecular dynamics, and so on, (b) use different dose metrics to explore whether these particle properties are suitable for quantifying the bioaccumulation and toxicity of NPs. For example, surface area (SA) and volume-specific surface area (VSSA) provide insights into the reactivity and biological interactions of NPs, which are critical for assessing the environmental and health impacts of NPs, and (c) increase the suite of NPs and organisms to verify the effectiveness of the EM algorithm-based mixture size distribution model established in this study.

CRediT authorship contribution statement

Yao Li: Writing – original draft, Methodology, Investigation. **Xiangrui Wang:** Investigation, Data curation. **Dingyuan Liang:** Investigation, Data curation. **Xiaoli Zhao:** Writing – review & editing. **Zhaomin Dong:** Writing – review & editing. **Yingchen Bai:** Writing – review & editing. **Wen-Xiong Wang:** Writing – review & editing. **Willie J.G.M. Peijnenburg:** Writing – review & editing. **Ying Wang:** Writing – review & editing, Investigation, Funding acquisition, Data curation. **Wenhong Fan:** Writing – review & editing, Methodology, Funding acquisition.

Declaration of competing interest

The authors declare that they have no known competing financial interests or personal relationships that could have appeared to influence the work reported in this paper.

Acknowledgments

This work was supported by the National Natural Science Foundation (Grant No. 42330710 and 42177240) and Beijing Natural Science Foundation (Grant No. 8242033) of China.

Supplementary materials

Supplementary material associated with this article can be found, in the online version, at doi:10.1016/j.aquatox.2025.107286.

Data availability

Data will be made available on request.

References

Abdolahpur Monikh, F., Chupani, L., Arenas-Lago, D., Guo, Z., Zhang, P., Darbha, G.K., Valsami-Jones, E., Lynch, I., Vijver, M.G., van Bodegom, P.M., Peijnenburg, W.J.G. M., 2021. Particle number-based trophic transfer of gold nanomaterials in an aquatic food chain. Nat. Commun. 12, 899.

Abdolahpur Monikh, F., Fryer, B., Arenas-Lago, D., Vijver, M.G., Krishna Darbha, G., Valsami-Jones, E., Peijnenburg, W.J.G.M., 2019. A dose metrics perspective on the association of gold nanomaterials with algal cells. Environ. Sci. Technol. Lett. 6, 732–738.

Ali-zade, R.A., 2008. Size distribution function of magnetite nanoparticles in disperse systems. Inorg. Mater. 44, 1105–1109.

Arnot, J.A., Gobas, F., 2006. A review of bioconcentration factor (BCF) and bioaccumulation factor (BAF) assessments for organic chemicals in aquatic organisms. Environ. Rev. 14, 257–297.

Avellan, A., Simonin, M., McGivney, E., Bossa, N., Spielman-Sun, E., Rocca, J.D., Bernhardt, E.S., Geitner, N.K., Unrine, J.M., Wiesner, M.R., Lowry, G.V., 2018. Gold nanoparticle biodissolution by a freshwater macrophyte and its associated microbiome. Nat. Nanotechnol. 13, 1072–1077.

Bai, Y., Wu, F., White, J.C., Xing, B., 2014. 100 nanometers: a potentially inappropriate threshold for environmental and ecological effects of nanoparticles. Environ. Sci. Technol. 48, 3098–3099.

Batley, G.E., Kirby, J.K., McLaughlin, M.J., 2013. Fate and risks of nanomaterials in aquatic and terrestrial environments. Acc. Che. Res. 46, 854–862.

Behra, R., Sigg, L., Clift, M.J.D., Herzog, F., Minghetti, M., Johnston, B., Petri-Fink, A., Rothen-Rutishauser, B., 2013. Bioavailability of silver nanoparticles and ions: from a chemical and biochemical perspective. J.R. Soc. Interface. 10, 20130396.

Benaglia, T., Chauveau, D., Hunter, D.R., Young, D.S., 2009. mixtools: an R package for analyzing mixture models. J. Stat. Softw. 32, 1–29.

Chen, X., Zhu, Y., Yang, K., Zhu, L., Lin, D., 2019. Nanoparticle TiO_2 size and rutile content impact bioconcentration and biomagnification from algae to *daphnia*. Environ. Pollut. 247, 421–430.

Cross, R.K., Tyler, C.R., Galloway, T.S., 2019. The fate of cerium oxide nanoparticles in sediments and their routes of uptake in a freshwater worm. Nanotoxicology 13, 894–908.

Dempster, A.P., Laird, N.M., Rubin, D.B., 1977. Maximum likelihood from incomplete data via the EM algorithm. J.R. Stat. Soc. Series B 39, 1–38.

Do, C.B., Batzoglou, S., 2008. What is the expectation maximization algorithm? Nat. Biotechnol. 26, 897–899.

Dowling, C.V., Cevaal, P.M., Faria, M., Johnston, S.T., 2022. On predicting heterogeneity in nanoparticle dosage. Math. Biosci. 354, 108928.

Eker, F., Duman, H., Akdaşçi, E., Bolat, E., Sarıtaş, S., Karav, S., Witkowska, A.M., 2024. A comprehensive review of nanoparticles: from classification to application and toxicity. Molecules 29, 3482.

Feng, Y., Liu, X., Huynh, K.A., McCaffery, J.M., Mao, L., Gao, S., Chen, K.L., 2017. Heteroaggregation of graphene oxide with nanometer- and micrometer-sized hematite colloids: influence on nanohybrid aggregation and microparticle sedimentation. Environ. Sci. Technol. 51, 6821–6828.

Ganguly, P., Breen, A., Pillai, S.C., 2018. Toxicity of nanomaterials: exposure, pathways, assessment, and recent advances. ACS Biomater. Sci. Eng. 4, 2237–2275.

Gao, C., Vuong, J., Zhang, Q., Liu, Y., Yin, Y., 2012. One-step seeded growth of Au nanoparticles with widely tunable sizes. Nanoscale 4, 2875–2878.

García-Álvarez, R., Hadjidemetriou, M., Sánchez-Iglesias, A., Liz-Marzán, L.M., Kostarelos, K., 2018. In vivo formation of protein corona on gold nanoparticles. The effect of their size and shape. Nanoscale 10, 1256–1264.

Gatoo, M.A., Naseem, S., Arfat, M.Y., Mahmood Dar, A., Qasim, K., Zubair, S., 2014. Physicochemical properties of nanomaterials: implication in associated toxic manifestations. Biomed. Res. Int., 498420

Gray, E.P., Coleman, J.G., Bednar, A.J., Kennedy, A.J., Ranville, J.F., Higgins, C.P., 2013. Extraction and analysis of silver and gold nanoparticles from biological tissues using single particle inductively coupled plasma mass spectrometry. Environ. Sci. Technol. 47, 14315–14323.

Hartenstein, V., Martinez, P., 2019. Phagocytosis in cellular defense and nutrition: a food-centered approach to the evolution of macrophages. Cell Tissue Res. 377, 527–547.

Jegatheesan, M., Bhattacharya, A., 2023. A model for nanoparticle transport and distribution with particle-interface interaction during binary alloy solidification. J. Cryst. Growth 610, 127173.

Lesniak, A., Salvati, A., Santos-Martinez, M.J., Radomski, M.W., Dawson, K.A., Åberg, C., 2013. Nanoparticle adhesion to the cell membrane and its effect on nanoparticle uptake efficiency. J. Am. Chem. Soc. 135, 1438–1444.

Lim, W.K., Denton, A.R., 2014. Polymer crowding and shape distributions in polymer-nanoparticle mixtures. J. Chem. Phys. 141.

Ma, J., Xia, D., Wang, Y., Niu, X., Jiang, S., Liu, Z., Guo, H., 2022. A comprehensive comparison among metaheuristics (MHs) for geohazard modeling using machine learning: insights from a case study of landslide displacement prediction. Eng. Appl. Artif. Intel. 114, 105150.

Markus, A.A., Krystek, P., Tromp, P.C., Parsons, J.R., Roex, E.W.M., Voogt, P.d., Laane, R.W.P.M., 2018. Determination of metal-based nanoparticles in the river Dommel in The Netherlands via ultrafiltration, HR-ICP-MS and SEM. Sci. Total Environ. 631-632, 485–495.

McColl, K.A., Vogelzang, J., Konings, A.G., Entekhabi, D., Piles, M., Stoffelen, A., 2014. Extended triple collocation: estimating errors and correlation coefficients with respect to an unknown target. Geophys. Res. Lett. 41, 6229–6236.

Mohanraj, V., Jayaprakash, R., Chandrasekaran, J., Robert, R., Sangaiya, P., 2017. Influence of pH on particle size, band-gap and activation energy of CdS nanoparticles

synthesized at constant frequency ultrasonic wave irradiation. Mater. Sci. Semicond. Process 66, 131–139.
Mortimer, M., Kasemets, K., Vodovnik, M., Marinšek-Logar, R., Kahru, A., 2011. Exposure to CuO nanoparticles changes the fatty acid composition of protozoa *Tetrahymena thermophila*. Environ. Sci. Technol. 45, 6617–6624.
Mortimer, M., Petersen, E.J., Buchholz, B.A., Orias, E., Holden, P.A., 2016. Bioaccumulation of multiwall carbon nanotubes in *Tetrahymena thermophila* by direct feeding or trophic transfer. Environ. Sci. Technol. 50, 8876–8885.
Park, M.V.D.Z., Neigh, A.M., Vermeulen, J.P., de la Fonteyne, L.J.J., Verharen, H.W., Briedé, J.J., van Loveren, H., de Jong, W.H., 2011. The effect of particle size on the cytotoxicity, inflammation, developmental toxicity and genotoxicity of silver nanoparticles. Biomaterials 32, 9810–9817.
Peijnenburg, W.J.G.M., Baalousha, M., Chen, J., Chaudry, Q., Von der kammer, F., Kuhlbusch, T.A.J., Lead, J., Nickel, C., Quik, J.T.K., Renker, M., Wang, Z., Koelmans, A.A., 2015. A review of the properties and processes determining the fate of engineered nanomaterials in the aquatic environment. Crit. Rev. Environ. Sci. Technol. 45, 2084–2134.
Quandt, R.E., Ramsey, J.B., 1978. Estimating mixtures of normal distributions and switching regressions. J. Am. Stat. Assoc.
Rajapakse, K., Drobne, D., Kastelec, D., Kogej, K., Makovec, D., Gallampois, C., Amelina, H., Danielsson, G., Fanedl, L., Marinsek-Logar, R., Cristobal, S., 2016. Proteomic analyses of early response of unicellular eukaryotic microorganism *Tetrahymena thermophila* exposed to TiO_2 particles. Nanotoxicology 10, 542–556.
Rees, P., Wills, J.W., Brown, M.R., Barnes, C.M., Summers, H.D., 2019. The origin of heterogeneous nanoparticle uptake by cells. Nat. Commun. 10.
Santás-Miguel, V., Arias-Estévez, M., Rodríguez-Seijo, A., Arenas-Lago, D., 2023. Use of metal nanoparticles in agriculture. A review on the effects on plant germination. Environ. Pollut. 334, 122222.
Schübbe, S., Schumann, C., Cavelius, C., Koch, M., Müller, T., Kraegeloh, A., 2012. Size-dependent localization and quantitative evaluation of the intracellular migration of silica nanoparticles in Caco-2 cells. Chem. Mater. 24, 914–923.
Sefcik, J., Grass, R., Sandkühler, P., Morbidelli, M., 2005. Kinetics of aggregation and gelation in colloidal dispersions. Chem. Eng. Res. Des. 83, 926–932.
Shang, W., Nuffer, J.H., Muñiz-Papandrea, V.A., Colón, W., Siegel, R.W., Dordick, J.S., 2009. Cytochrome c on silica nanoparticles: influence of nanoparticle size on protein structure, stability, and activity. Small 5, 470–476.
Summers, H.D., Gomes, C.P., Varela-Moreira, A., Spencer, A.P., Gomez-Lazaro, M., Pêgo, A.P., Rees, P., 2021. Data-driven modeling of the cellular pharmacokinetics of degradable chitosan-based nanoparticles. Nanomaterials 11, 2606.
Vidmar, J., Loeschner, K., Correia, M., Larsen, E.H., Manser, P., Wichser, A., Boodhia, K., Al-Ahmady, Z.S., Ruiz, J., Astruc, D., Buerki-Thurnherr, T., 2018. Translocation of silver nanoparticles in the *ex vivo* human placenta perfusion model characterized by single particle ICP-MS. Nanoscale 10, 11980–11991.
Wang, H., Han, X., Chen, Y., Guo, W., Zheng, W., Cai, N., Guo, Q., Zhao, X., Wu, F., 2021. Effects of F^-, Cl^-, Br^-, NO_3^-, and SO_4^{2-} on the colloidal stability of Fe_3O_4 nanoparticles in the aqueous phase. Sci. Total Environ. 757, 143962.
Wang, J., Jensen, U.B., Jensen, G.V., Shipovskov, S., Balakrishnan, V.S., Otzen, D., Pedersen, J.S., Besenbacher, F., Sutherland, D.S., 2011. Soft interactions at nanoparticles alter protein function and conformation in a size dependent manner. Nano Lett 11, 4985–4991.
Wang, J., Taaffe, M.R., 2015. Multivariate mixtures of normal distributions: properties, random vector generation, fitting, and as models of market daily changes. INFORMS J. Comput. 27, 193–203.
Wang, X., Liang, D., Wang, Y., Ma, Q., Xing, B., Fan, W., 2019. Effects of organic matter on uptake and intracellular trafficking of nanoparticles in *Tetrahymena thermophila*. Environ. Sci. Nano 6, 2116–2128.
Wray, A.T., Klaine, S.J., 2015. Modeling the influence of physicochemical properties on gold nanoparticle uptake and elimination by *Daphnia magna*. Environ. Toxicol. Chem. 34, 860–872.
Wu, Q., Shi, J., Ji, X., Xia, T., Zeng, L., Li, G., Wang, Y., Gao, J., Yao, L., Ma, J., Liu, X., Liu, N., Hu, L., He, B., Liang, Y., Qu, G., Jiang, G., 2020. Heterogenous internalization of nanoparticles at ultra-trace concentration in environmental individual unicellular organisms unveiled by single-cell mass cytometry. ACS Nano 14, 12828–12839.
Xiao, B., Zhang, Y., Wang, X., Chen, M., Sun, B., Zhang, T., Zhu, L., 2019. Occurrence and trophic transfer of nanoparticulate Ag and Ti in the natural aquatic food web of Taihu Lake, China. Environ. Sci. Nano 6, 3431–3441.
Xu, D., Knight, J., 2010. Continuous empirical characteristic function estimation of mixtures of normal parameters. Economet. Rev. 30, 25–50.
Xu, L., Jordan, M.I., 1996. On convergence properties of the em algorithm for gaussian mixtures. Neural Comput. 8, 129–151.
Zhang, L., Wang, W.-X., 2019. Dominant role of silver ions in silver nanoparticle toxicity to a unicellular alga: evidence from luminogen imaging. Environ. Sci. Technol. 53, 494–502.
Zhu, M., Nie, G., Meng, H., Xia, T., Nel, A., Zhao, Y., 2013. Physicochemical properties determine nanomaterial cellular uptake, transport, and fate. Acc. Chem. Res. 46, 622–631.